Crumpling of a Stiff Tethered Membrane

J. A. Åström,[1] J. Timonen,[2] and Mikko Karttunen[3]
[1]*Centre for Scientific Computing, P.O. Box 405, FIN-02101 Esbo, Finland*
[2]*Department of Physics, P.O. Box 35, FIN-40014 University of Jyväskylä, Finland*
[3]*Laboratory of Computational Engineering, Helsinki University of Technology, P.O. Box 9203, FIN-02015 HUT, Finland*
(Received 22 September 2003; published 8 December 2004)

A first-principles numerical model for crumpling of a stiff tethered membrane is introduced. This model displays wrinkles, ridge formation, ridge collapse, and initiation of stiffness divergence. The amplitude and wavelength of the wrinkles and the scaling exponent of the stiffness divergence are consistent with both theory and experiment. Close to the stiffness divergence further buckling is hindered by the nonzero thickness of the membrane, and its elastic behavior becomes similar to that of dry granular media. No change in the distribution of contact forces can be observed at the crossover, implying that the network of ridges is then *simultaneously* a granular force-chain network.

DOI: 10.1103/PhysRevLett.93.244301 PACS numbers: 46.25.−y, 05.70.Np, 68.60.Bs, 82.20.Wt

Crumpling of, e.g., sheets of paper, is an everyday phenomenon that one easily passes without much extra attention. In physics, however, crumpling has become a challenging topic of research. In addition to basic statistical mechanics properties [1], issues such as scaling of strength and energy [2,3], geometry and singularities [4,5], acoustic emission [6], and related phenomena in soft-matter systems [7] have become topics of interest. In this Letter, we present a first-principles numerical model for crumpling of a stiff tethered membrane, and relate the problem to the formation of force-chain networks in granular media [8,9].

Crumpling of a thin elastic sheet or a stiff membrane demands deformation energy. At very small strains, a membrane is uniformly compressed. Thin structures are, however, prone to buckling. At first, buckling appears as wrinkles or elliptical ridges. The wavelength and amplitude of the wrinkles depend on loading and on the dimensions of the membrane [10]. At constant strain the wavelength and amplitude of the ripples grow according to a unique scaling law [11,12]. As crumpling proceeds, the deformation energy begins to concentrate in narrow ridges and conical peaks [2,4], and eventually the strain there becomes so large that irreversible plastic yielding takes place. If the sheet is stretched out again, the ridge pattern can clearly be observed.

Another characteristic feature of the process is that the effective stiffness of the membrane increases fast with increasing degree of crumpling. The ultimate limit of crumpling would be to press the membrane into a volume equal to that of its own. In practice this limit cannot be reached. A ball that results from squeezing a piece of paper very hard contains about 75% air [13]. The effective stiffness of a membrane under crumpling has been found by careful experiments to display a power-law divergence in the dense-packing limit [13]. This divergence has been suggested to arise from the total ridge length diverging in this limit in a scale-invariant way.

In order to study wrinkles, ridge formation, and the effective stiffness in crumpled membranes, we constructed a numerical model for stiff tethered membranes. Our tethered membrane consisted of frictionless spheres with stiffness Y_s arranged in a triangular lattice. Each sphere had mass m and moment of inertia I, and was connected to its neighbors by massless elastic beams with both bending and tensile stiffness. We used a higher Young's modulus for the spheres (Y_s) than for the beams (Y_b). In the simulations reported here, we chose $Y_s = 10^7$ for spheres of radius 0.57. The beams had Young's modulus $Y_b = 5 \times 10^3$, length $1/\sqrt{3}$, and a square cross section of size 0.6^2. This implies a tensile modulus of 3.1×10^3 and a bending modulus of 3.7×10^2. The membrane had a thickness of ~ 0.6 and was placed horizontally (in the xy plane) in the middle of a rigid cube of time dependent size $X^3(t)$. Small random fluctuations in the z components of the spheres were introduced to avoid perfect symmetry, and the membrane was slightly broader in the y direction to allow initial wrinkles to form. Newtonian dynamics was applied.

The environment inside the box was strongly dissipative (as, e.g., a viscous fluid) such that a velocity dependent force $d \cdot \dot{\vec{x}}$ opposed the motion of spheres. The membrane dimensions were large enough for temperature fluctuations to be negligible. For computational reasons we did not include more than about 10^5 degrees of freedom in the system. Wrinkles and the onset of ridge formation were nevertheless observed, as well as the beginning of a power-law divergence of the effective stiffness with an exponent close to the experimental one. At low porosities the effective stiffness of the crumpled system deviates from the power law and behaves like that for a packing of solid spheres [14]. By separating the elastic-energy components in this limit, we found that the total ridge length indeed tended to diverge with zero critical porosity. The nonzero thickness of the membrane (~ 0.6) hindered the actual divergence, and a crossover to a different behavior took place in agreement with experiments.

Figure 1 shows a snapshot from a simulation that displays a few wrinkles at $t = 200$. Minimization of the elastic energy leads to an amplitude (A) to wavelength

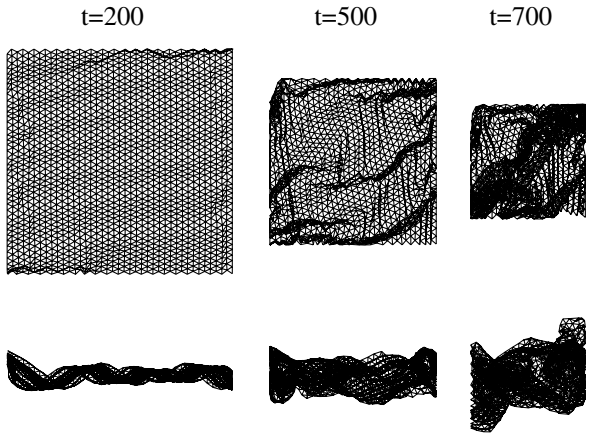

FIG. 1. Snapshots of a crumpling membrane: top views (above) and side views (below) for 3 times t. At $t = 200$ wrinkles are observed. At $t = 500$ ridges have begun to collapse. At $t = 700$ the membrane is entering the stiffness scaling regime, $(X - X_c)/X_c \approx 1.6$.

(λ) ratio for the wrinkles, $A/\lambda \sim (\Delta/W)^{1/2}$, with W the width and Δ the compression of the membrane perpendicular to the wrinkles [10]. This result is tested in Fig. 2(a) for our model membrane. The $A/\lambda \propto \Delta^{1/2}$ behavior holds up to $\Delta \approx 6$ (here $W \approx 23.4$). In Fig. 2(b) the scaling of λ as a function of dissipation coefficient d is compared to a theoretical prediction: d corresponds to the ''effective elastic foundation stiffness'' of Ref. [10]. (The λ of the wrinkles is determined by competition of bending stiffness and out-of-plane motion [10], and now the only force opposing this motion is damping.) For benchmarking, the time evolution of A is compared to the predicted scaling law, $A \sim t^{0.28}$ [11,12], in Fig. 2(c). In order to investigate λ, a long and narrow membrane was slowly compressed to a small strain that was then fixed. The time evolution thereafter of λ is shown in Fig. 2(d) together with the $t^{0.28}$ scaling.

Deformation of ridges in controlled geometries has been investigated both numerically and theoretically [2,3,5,15–20]. The elastic deformation energy of a ridge of length L scales as $\kappa(L/\delta)^{1/3}$, where δ is the thickness of the sheet and κ its bending modulus. Using this result, and following the derivation in Ref. [13], the scaling of membrane stiffness can be estimated. A crumpled sheet is divided into facets by the ridges. Ridges surrounding a facet of size L^2 have a length proportional to L, while it fills a space of size L^3. This leads to a bulk stiffness divergence, $K = -VdP/dV \propto V^{-11/3}$, when the volume of confinement V decreases under pressure P. This is not quite consistent with experimental findings. In Ref. [13], K was reported to scale as $K \propto (V_c - V)^{-\alpha}$ with $\alpha \approx 2.85$. Notice that this scaling relation can also be expressed as $F \propto (\phi_c - \phi)^{-\alpha+1}$ and $F \propto (X - X_c)^{-\alpha+1}$, where F is the external force, ϕ the solid-volume fraction, and $X(t)$ the time dependent linear dimension of the membrane.

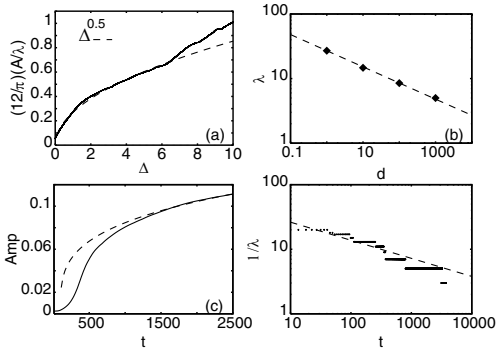

FIG. 2. (a) The ratio of amplitude to wavelength of the wrinkles A/λ as a function of membrane compression $\Delta = 0.02t$. The simulation result is compared to the predicted $A/\lambda \propto \sqrt{\Delta}$ [10]. (b) λ as a function of dissipation constant d. The simulation result is compared to the predicted $\lambda \propto d^{-1/4}$ [10]. (c) The time evolution of A at constant strain. The simulation result is compared to the predicted $A \propto t^{0.28}$ [11,12]. (d) The time evolution of λ at constant strain. The simulation result is compared to the predicted $1/\lambda \propto t^{-0.28}$ [11,12]. All predicted results are shown with a broken line. Figures 2(c) and 2(d) result from different simulations and the indicated times t are not comparable. The scaling regimes of A and λ appear simultaneously.

To investigate ridge formation in the simulations, we compared local bending to local energy. We used the sum of dot products of the nearest-neighbor bonds in the three principal directions of triangular lattice as a measure for local bending of the membrane,

$$p(\vec{x}, t) = \frac{1}{3}\sum_{i=1}^{3} \frac{\vec{l}_i^{\,n}(t) \cdot \vec{l}_i^{\,m}(t)}{l_i^n l_i^m}. \tag{1}$$

This was compared to the local elastic energies of the beams,

$$E_b(\vec{x}, t) = \sum_{i=1}^{6} \int_0^t \mathbf{F}(Y_b, \vec{x}(t)) d\vec{x}(t). \tag{2}$$

In Eq. (1), l^m and l^n are beam lengths on opposite sides of a lattice site. In Eq. (2), the elastic force $\mathbf{F}[Y_b, \vec{x}(t)]$ is inte-

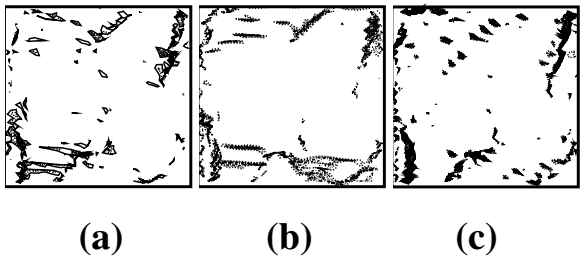

FIG. 3. Contour maps (at $t = 400$) of the spatial locations of (a) the highest local bendings $p(\vec{x}, t) < 0.6$, of (b) the highest elastic energies of the beams $E_b(\vec{x}, t)$, and of (c) the highest contact elastic energies of the spheres $E_s(\vec{x}, t)$.

grated over the related displacement, and the sum is over the six local degrees of freedom.

The elastic deformation energy of spheres in contact can also be used to identify ridges. This energy can be written as

$$E_s(\vec{x}, t) = \sum_{i=1}^{n} \frac{1}{2} Y_s \delta_s^2, \tag{3}$$

with δ_s the virtual "overlap" of spheres in contact. The sum is taken over all contacts.

Figure 3 shows contour plots of the lowest values of $p(\vec{x}, t)$ and the highest values of $E_b(\vec{x}, t)$ and $E_s(\vec{x}, t)$ at an early stage of the crumpling process ($t = 400$). It is obvious that E_b and E_s reach their highest values at locations of high local bending, and elongated structures, i.e., ridges, can clearly be seen. As crumpling proceeds, ridges grow and collapse, and the membrane folds. At later stages of crumpling it is not easy to detect ridges as the membrane profile becomes very complex.

The effective bulk stiffness of a membrane can be analyzed, e.g., by its stress-strain curve. The latter is the total force F on the confining box divided by the linear size of the membrane (F/W) as a function of $X(t)$. $F(t)/W$ increases fairly linearly before the membrane begins to buckle and fold. As the dense-packing limit is approached, F/W increases rapidly, until finally a saturation regime is entered.

Notice that there are three types of dense-packing limits: (1) For the tightest packing, the volume of the confining box equals that of the membrane, and the solid-volume fraction is $\phi_1 = 1.0$. (2) For hard-core spheres, the tightest packing is an fcc lattice with $\phi_2 = \pi\sqrt{2}/6 \approx 0.74$. (3) For a random dense-packing of spheres, $\phi_3 \approx 0.63$. For our model membrane, stiffness divergence takes place at $\phi_c \approx 0.75$, which is close to ϕ_2. This value was achieved for initial configurations close to that of a triangular lattice. Apart from very late phases of crumpling, the system may have some fcc type order, which explains the fairly high value of ϕ_c. (See also below.) Crossover to saturation behavior occurs, however, well before this ϕ_c is reached.

Figure 4(a) shows $F/(WY_s)$ for membranes with 10^4 and 4×10^4 degrees of freedom (simulations require about $10^6 - 10^7$ time steps). Simulation results are compared to the experimental result by Matan *et al.* [13], $F(X) \propto (X - X_c)^{-\alpha+1}$, with $\alpha \approx 2.85$. Good agreement is found until saturation sets in at $(X - X_c)/X_c \approx 0.03$. The critical values X_c were chosen so as to give the straightest lines in Fig. 4(a), and correspond to $\phi \approx 0.78$ and $\phi \approx 0.75$ for $W = 40$ and $W = 80$, respectively.

After saturation, stiffness behavior becomes different as beams no longer affect membrane stiffness. Instead, the membrane begins to resemble a granular packing. The stiffness of a 3D packing of solid spherical grains scales [14] like $(\phi - \phi_c)^\beta$, with $\beta \approx 1.62$ and a critical volume close to ϕ_3, $\phi_c \approx 0.63$, depending somewhat on the interaction between grains. Figure 4(b) shows a comparison between simulations and the scaling of $F(\phi)$ in these two regimes. The fairly high $\phi_c \approx 0.67$ is expected to result from deformation of spheres, which becomes non-negligible for high values of ϕ (hard-core spheres would be unstable numerically).

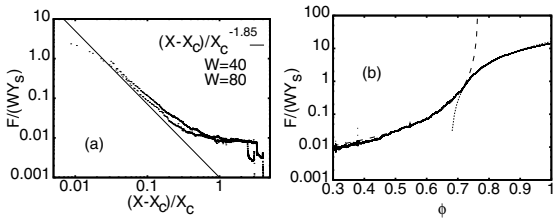

FIG. 4. (a) The total force F on the box around the membrane scaled by Y_s and linear membrane size W as a function of $(X - X_c)/X_c$. Data are shown for $W = 40$, 80. The solid line shows the experimental [13] power-law $F(X) \sim (X - X_c)^{-1.85}$. (b) $F/(WY_s)$ as a function of solid-volume fraction ϕ. The scaling of membrane stiffness, $(0.76 - \phi)^{-1.85}$, and of granular stiffness, $(\phi - 0.67)^{1.62}$, are compared to the simulation results.

By following the energy of the membrane from the initially flat to a fully crumpled state, it is possible to determine the energy component responsible for the stiffness divergence seen in Fig. 4. The external energy $\int_t F(t)dX(t)$ was also compared to the internal energy of the membrane, and the two were found to be equal, consistent with conservation of energy.

The internal energy can be split into five terms that are related to the force terms in the general equation of motion,

$$m\ddot{\vec{x}} + d\dot{\vec{x}} + \mathbf{K}\vec{x} + Y_s\vec{\delta}_s = \vec{f}_{\text{ext}}. \tag{4}$$

Here, x is the displacement, m the mass, d the damping coefficient, $\mathbf{K}$ the stiffness matrix, $\vec{\delta}_s$ the deformations (virtual overlap) of spheres in contact, and $\vec{f}_{\text{ext}}$ are forces applied on the walls of the confining box. The related energy terms are the following: (1) The elastic energy of the beams, E_b. (2) The compression energy at the contacts between spheres, E_s. (3) The compression energy of the spheres against external walls, $E_{\text{ext}} = 0.5 \sum Y_w \delta_w^2$. (4) The energy dissipated through damping, $E_d = \int_t \vec{F}_d d\vec{x}$. (5) The kinetic energy of the spheres, $E_m = 0.5 \sum m\dot{\vec{x}}^2$. The

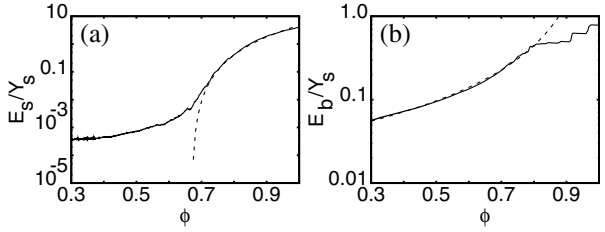

FIG. 5. (a) E_s as a function of ϕ. The broken line is $E_s \propto (\phi - 0.67)^{2.62}$. (b) E_b as a function of ϕ. The broken line is $E_b \propto (1 - \phi)^{-5/3}$.

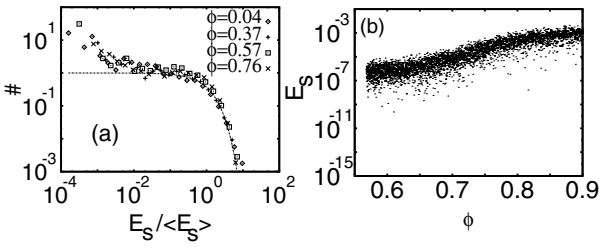

FIG. 6. (a) Distribution functions for the deformation energies at contacts between spheres for $\phi = 0.04, 0.37, 0.57, 0.76$. The data are compared to the equilibrium distribution $\exp(-E_s)$ [21]. (b) E_s as a function of ϕ. No crossover at $\phi \approx 0.72$ is visible.

dominating terms in the scaling regime are E_s and E_{ext}. The divergence of E_{ext} is rather trivial as it is just the deformation energy of the confining box. It is thus E_s that dominates the stiffness divergence. This explains to some extent why there is crossover to granular packings. When the deformation energy at the contacts between spheres dominates over the other energy terms, the beams no longer play a role in membrane stiffness.

If the membrane had no thickness, its folding would continue without limit. Then, according to the scaling arguments above, the energy related to deformation of beams would behave as $E_b \propto (\phi)^{5/3}$ at small ϕ. In analogy with Ref. [13], at high compression $1/\phi \to (1/\phi - 1/\phi_c)$. Setting $\phi_c = 1$, we obtain $E_b \propto [(1 - \phi)/\phi]^{-5/3}$. The two energy terms E_s and E_b, and their scaling behaviors, are compared in Fig. 5. (Notice that deformations of both beams and spheres are included in Fig. 4(b).)

Since there are two qualitatively different scaling behaviors of stiffness, one would expect a qualitative change at the crossover in the distribution of elastic energy or contact forces between spheres. We could not, however, detect any such change as demonstrated by the distributions shown in Fig. 6 for the deformation energies at the contacts. There was no change either at the crossover in the (changing) set of spheres that experienced the highest contact forces. This behavior strongly suggests that, at the crossover, ridges form the force chains of the granular-packing regime [8,9]. Notice that both are complicated 3D networks of essentially 1D lines of localized deformation energy. It is tempting to conclude that they are not separate phenomena, but different manifestations of a single phenomenon. The crossover would then be related to membrane thickness beginning to limit the density of network lines.

In conclusion, we have demonstrated that a numerical model of a tethered membrane can reproduce the theoretically predicted wrinkle and ridge formation and the experimentally observed stiffness divergence. The early-stage ridges can be traced by the elastic deformations of beams and the contact deformations of spheres. The divergence of the effective stiffness is initially dominated by bending and stretching of beams, and finally by the contact energy of spheres. When the solid-volume fraction is far below that of dense granular packings, the scaling of stiffness is "membranic," and when dense-packing is approached, it becomes "granular." There is no detectable change in the distribution of deformation energy when ridges turn into force chains.

[1] Y. Kantor, M. Kardar, and D. Nelson, Phys. Rev. Lett. **57**, 791 (1986).
[2] A. Lobkovsky, S. Gentges, H. Li, D. Morse, and T. A. Witten, Science **270**, 1482 (1995).
[3] B. A. DiDonna and T. A. Witten, Phys. Rev. Lett. **87**, 206105 (2001).
[4] E. Cerda, S. Chaïeb, F. Melo, and L. Mahadevan, Nature (London) **401**, 46 (1999).
[5] B. A. DiDonna, T. A. Witten, S. C. Venkataramani, and E. M. Kramer, Phys. Rev. E **65**, 016603 (2002).
[6] P. A. Houle and J. P. Sethna, Phys. Rev. E **54**, 278 (1996).
[7] E. Helfer, S. Harlepp, L. Bourieu, J. Robert, F. C. MacKintosh, and D. Chatena, Phys. Rev. Lett. **87**, 088103 (2001).
[8] C.-h. Liu, S. R. Nagel, D. A. Schecter, S. N. Coppersmith, S. Majumdar, O. Narayan, and T. A. Witten, Science **269**, 513 (1995).
[9] F. Radjai, M. Jean, J.-J. Moreau, and S. Roux, Phys. Rev. Lett. **77**, 274 (1996).
[10] E. Cerda and L. Mahadevan, Phys. Rev. Lett. **90**, 074302 (2003).
[11] D. Moldovan and L. Golubovic, Phys. Rev. Lett. **82**, 2884 (1999).
[12] D. Moldovan and L. Golubovic, Phys. Rev. E **60**, 4377 (1999).
[13] K. Matan, R. B. Williams, T. A. Witten, and S. R. Nagel, Phys. Rev. Lett. **88**, 076101 (2002).
[14] H. A. Makse, D. L. Johnson, and L. M. Schwartz, Phys. Rev. Lett. **84**, 4160 (2000).
[15] B. A. DiDonna, Phys. Rev. E **66**, 016601 (2002).
[16] E. M. Kramer and T. A. Witten, Phys. Rev. Lett. **78**, 1303 (1997).
[17] A. E. Lobkovsky and T. A. Witten, Phys. Rev. E **55**, 1577 (1997).
[18] E. Cerda and L. Mahadevan, Phys. Rev. Lett. **80**, 2358 (1998).
[19] S. Chaïeb and F. Melo, Phys. Rev. E **60**, 6091 (1999).
[20] See EPAPS Document No. E-PRLTAO-93-076542 for a figure of a stretching ridge in a folded membrane, the strain along the ridge as function of folding time (t) and the scaling of stretching energy (W) as function of ridge length (L). A direct link to this document may be found in the online article's HTML reference section. The document may also be reached via the EPAPS homepage (http://www.aip.org/pubservs/epaps.html) or from ftp.aip.org in the directory /epaps/. See the EPAPS homepage for more information.
[21] C. S. O'Hern, S. A. Langer, A. J. Liu, and S. R. Nagel, Phys. Rev. Lett. **88**, 075507 (2002).